PAPER

Investigation on the promotional role of Ga_2O_3 on the CuO–ZnO/HZSM-5 catalyst for CO_2 hydrogenation†

Jie Du, Yajing Zhang, ID * Kangjun Wang,* Fu Ding, Songyan Jia, ID Guoguo Liu and Limei Tan

Dimethyl ether (DME) can be directly synthesized from carbon dioxide and hydrogen by mixing methanol synthesis catalysts and methanol dehydration catalysts. The activity and selectivity of the catalyst can be greatly affected by the promoter; herein, we presented a series of CuO–ZnO–Ga_2O_3/HZSM-5 hybrid catalysts, which were prepared by the coprecipitation method. The effect of the Ga_2O_3 content on the structure and performance of the Ga-promoted Cu–ZnO/HZSM-5 based catalysts was thoroughly investigated. The results showed that the addition of Ga_2O_3 significantly increased specific surface areas and Cu areas, decreased the size of Cu particles, maintained the proportion of Cu^+/Cu^0 on the surface of the catalyst, and strengthened the metal–support interaction, resulting in high catalytic performance.

1. Introduction

Recently, human beings mainly have two concerns, global warming and energy shortage.[1] CO_2 is one of the main greenhouse gases and is considered the main contributor to global warming.[2] The hydrogenation of CO_2 to other chemicals (hydrocarbons, methanol, and dimethyl ether (DME)) can effectively solve these problems. Particular attention has been paid to the synthesis of DME. DME may be used as an alternative fuel and is widely used as feedstock for the production of aerosols, refrigerants, foaming agents, *etc.*[3,4]

One-step CO_2 hydrogenation to dimethyl ether combines two successive steps of methanol synthesis and methanol dehydration over a hybrid catalyst in a single reactor. The catalyst is composed of a methanol synthesis component[5] and methanol dehydration component together;[6] in some cases, the catalyst is also called a bifunctional/hybrid catalyst.[7,8] The Cu–ZnO/HZSM-5 based catalyst has been considered as an optimum combination of the two components, and the active temperature of both components is within the same temperature range.[9,10] At present, however, the hydrogenation of CO_2 to DME still has a low CO_2 conversion and a low selectivity to DME over the catalyst. Various methods were employed to modify its composition and structure, aiming to enhance the performance. For example, optimization methods include modifying

methanol dehydration catalysts,[11] changing the preparation process of catalysts,[12] adopting a core–shell structure[13] and mixing with new catalysts.[14]

Previous studies have shown that appropriate promoters can effectively improve the performance of Cu–ZnO/HZSM-5 with optimized composition. Many studies have been performed on catalysts for the hydrogenation of CO_2 to dimethyl ether, with carriers,[15] promoters,[7,16] *etc.*, aiming to increase the catalytic performance of catalysts.

Ga_2O_3, as a promoter, has been used by some researchers in CO_2 conversion catalysts.[17–19] In comparison, research has rarely been reported on dimethyl ether catalysts[20,21] and there are fewer researchers who have studied the influence of Ga_2O_3 content changes on catalysts. In the present work, we found that Ga_2O_3 can significantly improve the selectivity and yield of dimethyl ether; the effects of Ga_2O_3 content on the performance and structure of the CuO–ZnO/HZSM-5 catalyst were carefully investigated in direct DME synthesis from a CO_2 and H_2 mixture.

2. Experimental section

2.1 Catalyst preparation

The catalysts were prepared by the oxalate co-precipitation method, and the mass ratio of the CuO–ZnO–Ga_2O_3 component to HZSM-5 (Catalyst Plant of Nankai University, SiO_2/Al_2O_3 = 38, molar ratio) was 2 : 1.[16] First, a certain amount of analytically pure nitrate precursors $Cu(NO_3)_2$, $Zn(NO_3)_2$, and $Ga(NO_3)_3$ was dissolved into a certain amount of ethanol (denoted as solution A; the total molar concentration is 1 mol L^{-1}); $H_2C_2O_4 \cdot 2H_2O$ (200 wt% of metal nitrate) was also dissolved into ethanol (solution B, 1 mol L^{-1}). Second, parallel

College of Chemical Engineering, Shenyang University of Chemical Technology, Shenyang 110142, PR China. E-mail: yjzhang2009@163.com; angle_79@163.com; Tel: +86-24-89383902

† Electronic supplementary information (ESI) available: Experimental section, figures and tables given in the Results and discussion section. See DOI: 10.1039/d0ra10849a

solutions A and B were slowly dropped into a beaker containing HZSM-5 ethanol solution and kept under stirring at 60 °C. The suspension was sealed and aged for 2 hours and then the ethanol was evaporated at 80 °C to get a precipitate. Finally, the precipitate was dried at 120 °C for 12 hours and calcined in air at 400 °C for 4 hours. The powder of the CZG$_x$H catalyst was ground, pressed, pulverized and sieved to obtain particles of 20 to 40 mesh before the activity was tested. The Ga$_2$O$_3$ modified CuO–ZnO/HZSM-5 (CuO : ZnO = 7 : 3, mass ratio) catalysts were abbreviated as CZG$_x$H (x stands for theoretical Ga$_2$O$_3$/CZ wt%).

2.2 Catalyst testing

Catalyst testing was carried out in a continuous-flow fixed-bed reactor made of stainless steel (i.d. = 10 mm). First, the catalyst was reduced with 10% H$_2$/N$_2$ at 300 °C for 3 h under atmospheric pressure. Then it was cooled to 50 °C and reactant gas flow was introduced, raising the pressure to 3.0 MPa, and the reaction temperature was 260 °C. The exit line was heated to prevent condensation. The products were analyzed on line with a gas chromatograph (SP-3420) equipped with both a TCD (for CO and CO$_2$, GDX-101 connected with Porapak T column) and a FID (for CH$_4$, CH$_3$OH and CH$_3$OCH$_3$, Porapak Q column). Conversion and selectivity values were calculated by the internal standard and mass conservation method.

2.3 Catalyst characterization

XRD measurements were performed on a Rigaku D/max 2500pc X-ray diffractometer with Cu-Kα radiation ($l = 1.54156$ Å) at a scan rate of 4° min^{-1} at 50 kV and 250 mA. The crystallite size was calculated using Scherrer's equation. Copper surface areas (S_{Cu}) were measured by a nitrous oxide titration method as described elsewhere.[22]

BET surface areas were measured by N$_2$ adsorption at −196 °C using a Quantachrome Autosorb 1-C. Before the absorption–desorption measurements, samples were degassed under vacuum at 300 °C for 3 h. The specific BET (S_{BET}) was estimated from the linear part of the Brunauer–Emmett–Teller (BET) plot.

H$_2$-TPR of catalysts was performed on a chemisorption analyser (ChemBET 3000). Before reduction, 0.02 g of sample was preheated with flowing He at 400 °C for 60 min, and then cooled down to room temperature. Subsequently, the temperature was raised in 10% H$_2$/Ar (50 mL min^{-1}) at a ramp rate of 10 °C min^{-1} to 400 °C. H$_2$ consumption was detected with a TCD.

NH$_3$-TPD was conducted on a ChemBET 3000. 300 mg catalyst was heated to 400 °C for 30 min, and then cooled to 50 °C; following that 6 vol% NH$_3$/Ar was introduced for adsorption (60 min). Then, the catalyst was flushed with a He stream (30 mL min^{-1}) for 60 min to remove the weakly adsorbed NH$_3$, and finally it was heated from 50 to 800 °C at a rate of 10 °C min^{-1}. The NH$_3$-TPD signal was recorded.

CO$_2$-TPD was also conducted on a ChemBET 3000. 50 mg catalyst was first reduced at 300 °C in a H$_2$ flow of 30 mL min^{-1} for 1 h, purged with purified Ar, and further treated at 450 °C for

0.5 h in Ar. After cooling to 40 °C, CO$_2$ adsorption was switched to saturation, and then the catalyst was flushed with a He stream (30 mL min^{-1}) for 60 min, and finally it was heated from 50 to 900 °C at a rate of 10 °C min^{-1}. The CO$_2$-TPD signal was recorded.

X-ray photoelectron spectroscopy (XPS) and X-ray-induced Auger electron spectroscopy were performed on an ESCALAB 250Xi spectrometer. The monochromatized Al-Kα beam (1486.8 eV) was used as an X-ray source to confirm the characteristic peaks of Cu 2p, Zn 2p, Ga 2p, and C 1s with a beam resolution of 0.1 eV. The characteristic C–C peak at 284.6 eV assigned to C 1s was further used as a reference peak.

3. Results and discussion

3.1 Catalytic performance of the catalysts

In Table 1, the catalytic performances of the CZG$_x$H catalysts are displayed, along with the behaviour of a Ga$_2$O$_3$-free sample (CZG$_0$H) taken as a reference. In this reaction, DME was the main product, while methanol, CO and trace hydrocarbons (methane, ethane, *etc.*) were identified as by-products. Apparently, the catalytic performance is significantly improved with the addition of Ga$_2$O$_3$ compared to the Ga$_2$O$_3$-free catalyst under the same reaction conditions. All the Ga$_2$O$_3$-added catalysts exhibited higher CO$_2$ conversion (Fig. S1†) and higher selectivity to DME (Fig. S2†). On the other hand, it is also observed that the CO$_2$ conversion, DME selectivity and DME yield show a trend of increase initially, followed by a decrease with Ga$_2$O$_3$ addition; the attained better catalytic performances were respectively 22.3%, 62.6% and 14.0% over the CZG$_5$H catalyst. By comparing the catalysts in this paper with similar material catalysts with similar ratios in other literature under almost the same test conditions,[23] although there is no significant difference between the catalysts with promoters Ga$_2$O$_3$ and ZrO$_2$ in terms of the carbon dioxide conversion, the selectivity to dimethyl ether of the Ga$_2$O$_3$ modified catalyst was significantly higher than that of the ZrO$_2$ modified catalyst, so the yield of dimethyl ether is improved accordingly. The catalytic performance results showed that an appropriate amount of Ga$_2$O$_3$ could effectively convert CO$_2$ into dimethyl ether, but not in excess. In order to evaluate the influence of Ga$_2$O$_3$ on the catalysts, the catalysts were further characterized in the following sections.

Turnover frequency (TOF) of CO$_2$, which represents the molecular number of the transferred CO$_2$ per second per surface Cu atom, has been calculated from the S_{Cu} for various catalysts. As shown in Fig. 1, to better understand the role of metallic Cu in the process of hydrogenation of CO$_2$, TOF is also plotted *versus* S_{Cu} of the CZG$_x$H catalysts. It can be seen that the values of TOF varied in the range of 0.67–0.75 × 10^{-3} s^{-1}. TOF is not a fixed value, which indicates that the catalytic activity is not only related to S_{Cu}, but also affected by such factors as the interaction between copper and zinc oxide.[24] This observation indicates a good correlation of structure sensitive characters of DME from CO$_2$.[25] In addition, combining the values of TOF with the results of Ga$_2$O$_3$ content in Table 1 indicates that the addition of Ga$_2$O$_3$ can increase the value of TOF.

Table 1 Physicochemical properties and catalytic performances of the catalysts

Catalyst	S_{BET} (m² g⁻¹)	Dispersion[a] (%)	$S_{Cu}{}^{a}$ (m² g⁻¹)	$d_{Cu}{}^{a}$ (nm)	CO_2 conversion[b] (%)	Selectivity[b] (%)				DME yield[b] (%)
						CO	C_2H_4	MOH	DME	
CZG$_0$H	123.7	13.2	33.4	7.6	18.6	49.5	1.9	5.0	43.7	8.1
CZG$_1$H	146.1	14.5	36.6	6.9	19.9	41.4	2.1	3.7	52.8	10.5
CZG$_3$H	154.2	15.0	37.9	6.7	20.8	34.8	2.0	4.9	58.3	12.1
CZG$_5$H	163.8	15.5	39.1	6.5	22.3	30.0	2.0	5.5	62.6	14.0
CZG$_{10}$H	164.2	15.3	38.5	6.6	21.3	31.5	2.1	5.8	60.7	13.0

[a] Determined by the nitrous oxide titration method. [b] Reaction conditions: $T = 260\ °C$, $P = 3.0$ MPa, weight = 1 g, $CO_2 : H_2 : N_2 = 3 : 9 : 1$, GHSV = 1500 h⁻¹.
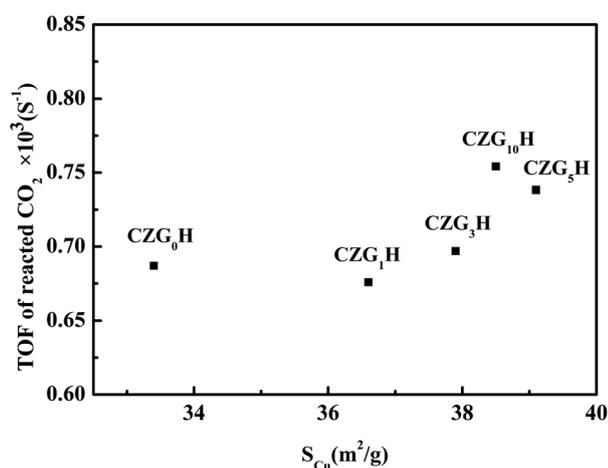
Fig. 1 The relationship between the TOF of reacted CO_2 and the surface copper areas (S_{Cu}).

3.2 The structure of the catalysts

The X-ray diffraction results are shown in Fig. 2. For all the catalysts, the diffraction peaks at $2\theta = 35.5°$, $38.7°$, $48.6°$, $58.3°$, $68.1°$, and $75.2°$ can be indexed to the CuO phase (tenorite, JCPDS 48-1548), the peaks at $2\theta = 31.8°$, $34.4°$, $36.3°$, $47.6°$, $56.6°$, $62.9°$, $66.4°$, and $72.6°$ can be ascribed to the ZnO phase (JCPDS 65-3411), and the diffraction peaks observed in the 2θ range of 21–25° can be attributed to HZSM-5 (JCPDS 44-0003). However, diffraction peaks belonging to Ga_2O_3 or other new binding products are not observed for the catalysts with the promoter of Ga_2O_3 added, indicating that Ga_2O_3 species are present in either the amorphous state or highly dispersed in the catalysts and cannot be detected by XRD.[26] Strong CuO peak intensities were detected in all the catalysts, which confirmed that they had been completely crystallized. With the increase of Ga_2O_3 content to 5%, the intensities of the CuO diffraction peaks decreased gradually, whereas the peak width broadened slightly; it can be inferred from Scherrer's formula that the average particle size of CuO decreases, indicating that the crystallinity of CuO decreased and the dispersion of copper increased with the addition of Ga_2O_3. Some diffraction peaks of CuO ($2\theta = 35.5°$) and ZnO ($2\theta = 34.4°$ and $36.3°$) were severely superimposed on each other, and similar phenomena had

appeared in other works,[27] which shows that the embedded dispersion of CuO and ZnO are relatively uniform. The fine particles of CuO and ZnO which may exist in an amorphous or more disordered form, this will promote the synergistic effect, thus resulting in the intensified CuO–ZnO interaction.[28] This interaction between CuO and ZnO is beneficial to the increases in the activity for CO_2 conversion, which exactly coincides with catalytic performance results.

The Cu surface area, Cu dispersion, and Cu particle sizes are greatly affected by the concentrations of Ga_2O_3, as listed in Table 1. When the content of Ga_2O_3 increased, the change of the peak shape first increased and then decreased appeared in the Cu surface area and Cu dispersion. The Cu surface area correlated well with the copper dispersion; the results showed higher values of S_{Cu} and D_{Cu} for CZG$_5$H than other catalysts, and the maximum values were found to 39.1 (m² g⁻¹) and 15.5%, respectively, while the particle size trend was opposite. The small CuO particles and improved copper dispersion can be ascribed to the character of the structural promoter of Ga_2O_3 increasing the resistance of CuO to sinter during the thermal treatment,[30] which consequently results in a larger Cu surface
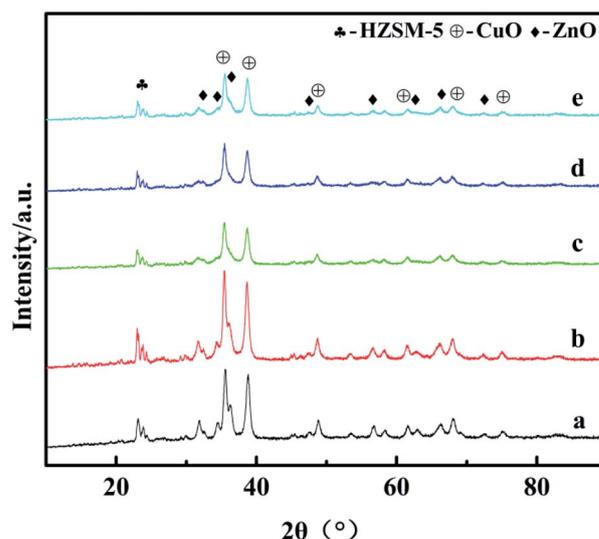
Fig. 2 XRD patterns of the catalysts: (a) CZG$_0$H; (b) CZG$_1$H; (c) CZG$_3$H; (d) CZG$_5$H; (e) CZG$_{10}$H.
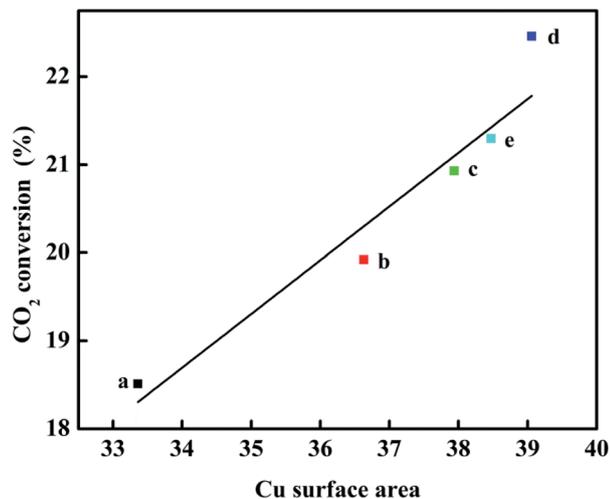
Fig. 3 Relationship between the CO_2 conversion and Cu surface area.

area of the CZG_xH catalysts. Decreasing the Ga_2O_3 loading below 5% or increasing the Ga_2O_3 loading over 5% also resulted in a decrease in Cu surface area and Cu dispersion, and an increase in Cu particle size, which is consistent with the XRD results. The results confirmed the conclusion that adding excessive Ga_2O_3 is no longer beneficial to improve the dispersion of Cu on the catalyst surface. As displayed in Fig. 3, a plot of CO_2 conversion as a function of Cu surface area is depicted, and there is a linear relationship between them. Perhaps an increase in the S_{Cu} resulted in more dissociatively adsorbed hydrogen and its migration to ZnO or Ga_2O_3 through hydrogen spillover, which improved the activity of the catalyst. Therefore, Cu surface area is a crucial factor for the high yield of DME by hydrogenation of CO_2.

3.3 The reducibility of the catalysts

It has been reported that ZnO and Ga_2O_3 are not reduced under the H_2-TPR conditions; therefore, the H_2 reduction peaks
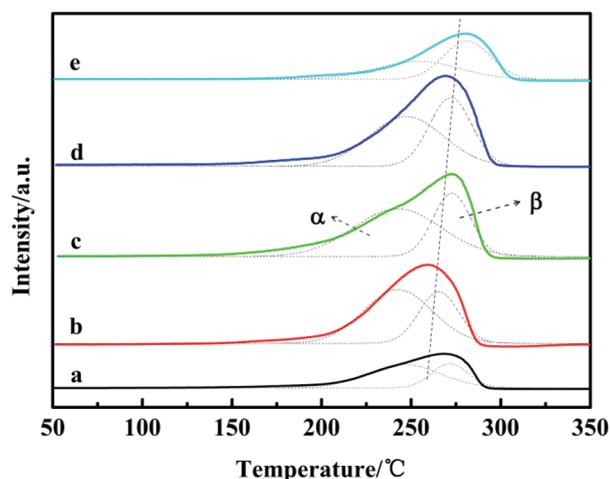
Fig. 4 H_2-TPR profiles of the catalysts: (a) CZG_0H; (b) CZG_1H; (c) CZG_3H; (d) CZG_5H; (e) $CZG_{10}H$.

Table 2 Peak temperature, peak area and distribution ratio of H_2-TPR

Catalyst	T_α	T_β	$A_\alpha + A_\beta$	$A_\alpha/(A_\alpha + A_\beta)$ (%)
CZG_0H	236	269	6282	53
CZG_1H	238	264	14463	57
CZG_3H	241	270	15694	63
CZG_5H	246	272	15849	69
$CZG_{10}H$	248	277	8107	30

observed were only related to the CuO reduction. The H_2-TPR results are presented in Fig. 4. The occurrence of two Gaussian fitting peaks (α and β) is observed for all of the H_2-TPR profiles, which has been related to the reduction of different CuO species in the catalysts. Previous authors have observed similar reduction peaks for Cu based catalysts and have regarded the α reduction peak at about 220–250 °C as the surface reduction peak of dispersed amorphous CuO, whereas the β reduction peaks around 270–300 °C can be classified as the reduction peaks of CuO in the bulk phase with large grains.[31]

In Table 2, it is notable that the reduction peaks of all Ga_2O_3-added catalysts shifted to the higher temperature region, consistent with other literature studies.[32] This is due to the existence of CuO particles with different sizes and the different interaction strength between CuO particles and other oxides in the catalyst.[17] As the content of Ga_2O_3 changes, the area ratio of the two Gaussian peaks also changes. Among them, $A_\alpha/(A_\alpha + A_\beta)$ of CZG_5H is the largest, the proportion of easily reduced CuO on the surface is up to 69% in this catalyst system, and the more CuO on the surface is beneficial to the hydrogenation of CO_2. Whether the amount of Ga_2O_3 is too large or too small, the value of $A_\alpha/(A_\alpha + A_\beta)$ will decrease. Moreover, it could be observed that the addition of Ga_2O_3 (<5%) significantly increased the peak areas as compared to the reduction peak area of the Ga_2O_3-free catalyst, indicating that more CuO in the catalysts is reduced to produce more hydrogen consumption. However, adding excess Ga_2O_3 (10%) leads to a lower peak area; this suggests that Ga_2O_3 species may be incorporated into CuO or may be deposited on the surface of CuO, in accordance with previous observations.

3.4 Surface acidity of the catalysts

Fig. 5 shows the NH_3-TPD profiles of the catalysts. There are three desorption peaks near 110–150 °C (peak α), 330–400 °C (peak β) and 400–500 °C (peak γ) on the surface of each catalyst, which respectively correspond to the weak acid center, medium acid center and strong acid center on the surface of the catalyst.[33] In Table 3, compared with the Ga_2O_3-free catalyst, peak α moves slightly to higher temperature, while peaks β and γ shift to higher temperature more obviously, suggesting the increased strength, implying that Ga_2O_3 modification increased the catalyst medium and strong acidity obviously. During the preparation process, the amount of oxalic acid as a precipitator will be changed with the addition of Ga_2O_3, which may modify the medium and strong acid sites. Comparing the total amount
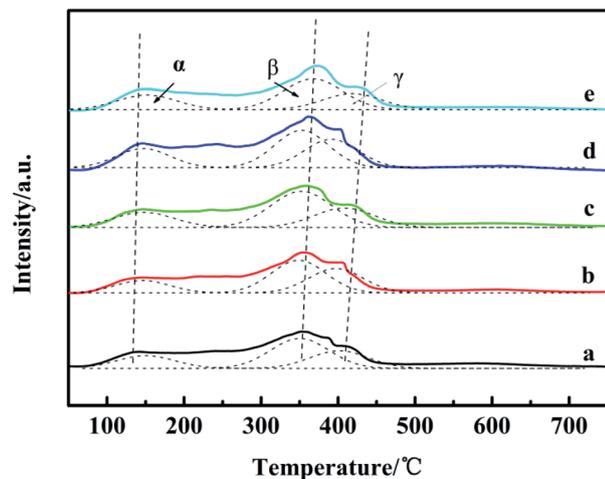
Fig. 5 NH_3-TPD spectrum of catalysts with different Ga_2O_3 contents: (a) CZG_0H; (b) CZG_1H; (c) CZG_3H; (d) CZG_5H; (e) $CZG_{10}H$.

Fig. 6 Spectra of the prepared hybrid catalysts of CZG_0H and CZG_5H: (A) Cu 2p; (B) Zn 2p; (C) Ga 2p.

of acid with the increase of Ga_2O_3 content in the catalyst, the peak areas of NH_3 desorption peaks first increase and then decrease, indicating that the surface acid amounts change correspondingly.[34] It can be seen that the peak area of CZG_5H is the largest, and the content of weak acids is large, which is beneficial to the improvement of DME selectivity.[17,33] Comparing the NH_3-TPD and the previous catalytic performance results (Table 1), the CZG_xH with different Ga_2O_3 contents has similar methanol selectivity, which indicates that the acidity of the catalyst is enough to convert the generated methanol to DME. The dimethyl ether selectivity is significantly different. The results suggest that an appropriate acid content and acid strength of the catalyst are favorable for the selectivity to DME in the reaction of CO_2 hydrogenation to dimethyl ether.

3.5 Adsorption and desorption performance of catalysts for CO_2

CO_2 TPD profiles of reduced CZG_0H and CZG_5H catalysts are shown in Fig. S3.† There are three CO_2 desorption peaks. With Ga_2O_3 addition, the proportion of weak CO_2 adsorption (<300 °C) and strong CO_2 adsorption (>500 °C) increased, while the proportion of medium adsorption (300–450 °C) decreased. It can be seen that the addition of Ga_2O_3 did not promote the absorption of CO_2 (Fig. S3 and Table S5†).

3.6 X-ray photoelectron spectroscopy analysis

As shown in Fig. 6, the surface chemical states of the Cu, Zn and Ga on the prepared catalysts were analyzed by X-ray photoelectron spectroscopy (XPS). As representative results, the XPS spectra of Cu 2p for the *ex situ* prepared catalysts of CZG_0H and CZG_5H are shown in Fig. 6A. It can be observed that the binding energies (BE) of the main characteristics peaks at about 932.9 eV and 953.0 eV are assigned to Cu $2p_{3/2}$ and Cu $2p_{1/2}$, respectively,[35] and two shake-up satellite peaks appeared at 940–945 eV, indicating that the copper species in the catalyst surface existed in the form of CuO.[36] In addition, the binding energy values of Cu $2p_{3/2}$ and cu $2p_{1/2}$ increased slightly with the addition of Ga_2O_3, indicating that the interaction between Cu and Ga was enhanced,[37] which was consistent with the results of H_2-TPR. Both of the spectra contained two peaks at about 1022 and 1045 eV (Fig. 6B), which are assigned to Zn $2p_{3/2}$ and Zn $2p_{1/2}$ peaks of ZnO,[38] respectively, with a spin energy separation of 23 eV. This shows that zinc atoms are present in the catalyst in the form of ZnO.[39] The binding energies of Zn $2p_{1/2}$ and Zn $2p_{3/2}$ become larger with the addition of Ga_2O_3. Similarly, as shown in Fig. 6C, the double peaks of 1117.4 eV and 1144.5 eV correspond to the binding energies of Ga $2p_{3/2}$ and Ga $2p_{1/2}$ of

Table 3 The acid properties of catalysts with different Ga_2O_3 contents[a]

Catalyst	Weak acidic amount	Medium acidic amount	Strong acidic amount	Total acidic amount
CZG_0H	0.13 (140 °C)	0.32 (354 °C)	0.19 (407 °C)	0.64
CZG_1H	0.13 (144 °C)	0.34 (355 °C)	0.25 (409 °C)	0.71
CZG_3H	0.20 (148 °C)	0.47 (356 °C)	0.25 (415 °C)	0.92
CZG_5H	0.22 (146 °C)	0.44 (362 °C)	0.34 (415 °C)	1.00
$CZG_{10}H$	0.19 (152 °C)	0.39 (373 °C)	0.21 (425 °C)	0.79

[a] The amount of acidity of CZG_5H was assigned as 1.0, and compared with that of the other samples. The temperature in parentheses is T_{max}.

Fig. 7 Spectra of the reduced and recovered CZG_0H and CZG_5H hybrid catalysts: (A) Cu 2p; (B) Cu (LMM) Auger; (a) the reduced CZG_0H; (b) the recovered CZG_0H; (c) reduced CZG_5H; (d) the recovered CZG_5H.

reduced CZG_5H, respectively, indicating that Ga_2O_3 is in the oxidation state of Ga^{3+}.[40]

The XPS spectra of reduced and recovered CZG_0H and CZG_5H hybrid catalysts are shown in Fig. 7. The signal peaks of Cu that appeared at 933 eV and 952 eV are assigned to Cu $2p_{3/2}$ and Cu $2p_{1/2}$, respectively, which correspond to the reduction sites (Cu^0 and/or Cu^+)[41] (Fig. 7A). Compared with Fig. 6A, the Cu 2p XPS spectra of the catalyst after H_2 reduction show that the satellite peak disappeared and the Cu 2p peak moved to lower binding energy at the same time, indicating that copper was almost reduced to Cu^+ or Cu^0.[42] The enhanced peak intensity indicates that the copper part of the bulk phase migrates to the surface during reduction. Sun *et al.* proposed that the electronic interaction between Cu and Zn will produce the active center Cu^+–O–Zn, which provides a synergistic effect between Cu and ZnO for the production of dimethyl ether.[43] After the reaction, the XPS intensity of Cu 2p changed slightly, but no obvious changes in the position and shape were observed. It can be seen that the valence state of copper has not changed after the catalyst is used (10 hours). The comparison shows that the valence states of Cu at the main Cu $2p_{3/2}$ and Cu $2p_{1/2}$ on the catalyst surface are basically unchanged after reduction and reaction, indicating that the catalyst has good chemical stability as a whole. In the XPS spectra of Cu $2p_{3/2}$, the binding energies of Cu^+ and Cu^0 are almost the same, and those of Cu_2O and Cu metal are 932.2 eV and 932.4 eV, respectively. Therefore, the kinetic energies (KE) of the reduced catalyst were studied by Cu LMM X-ray auger electron spectroscopy (XAES) spectrum analysis to further distinguish the valence state of Cu on the catalyst surface. The line positions in the Cu (LMM) Auger spectra of the reduced and recovered CZG_0H and CZG_5H catalysts indicate that the two asymmetrically located peaks near 916.5 eV and 918.7 eV correspond to Cu^+ and Cu^0 species,[18] respectively, and Cu^+ is the main copper species detected on the catalyst surface (Fig. 7B). Based on the corresponding Cu LMM peaks, the Cu^+/Cu^0 area ratios of the two reduction catalysts are obtained by calculation. The area ratio of the CZG_5H catalyst was higher than that of the CZG_0H catalyst, which indicated that the ratio of Cu^+/Cu^0 can be maintained better with the addition of Ga_2O_3 and the activity of the catalyst may be determined by Cu^+ species rather than Cu^0 species.[44] It is worth noting that this XPS test is not performed *in situ*, and this may be subject to some errors. Although there is still controversy about the active center of copper-based catalysts in the process of CO_2 hydrogenation to

methanol, it is generally believed that Cu^+ and Cu^0 contribute to the catalytic activity.[19]

3.7 Effect of reaction temperature on the catalysts

Reaction temperature also has a significant effect on CO_2 conversion, product selectivity and yield. Under different temperature conditions, the changes of conversion and yield are shown in Fig. 8. It has been reported in the literature that Cu/ZnO-based catalyst activity will be reduced when the temperature exceeds 300 °C; the deactivation is caused by the aggregation of Cu crystals.[45] Therefore, the maximum temperature we tested was controlled at 300 °C. Comparing the curves at different temperatures, it is concluded that the optimal reaction temperature is 260 °C. At low temperature, there is competitive adsorption of the reaction product CO and reactant CO_2 on metal active sites. Methanol is mainly prepared by hydrogenation of CO produced by the reverse reaction of water vapor, so the conversion of carbon dioxide is low. Since the reaction is exothermic, with the increased temperature and reaction time of HZSM-5, there will be carbon deposition on the outer surface and in the channel, leading to a decrease in the DME selectivity. In addition, higher temperatures will cause sintering and crystallization of copper species, causing catalyst coking and thereby reducing the conversion rate of carbon dioxide.[15] The yield of DME reached the maximum at 260 °C, which means that due to the exothermic reaction, the conversion of CO_2 is thermodynamically restricted, or may be Cu sintering.[46] Relatively the selectivity of CO gradually increased, which is due to the reverse water vapor reaction (RWGS) of CO_2.[47] In view of these results, we investigated the CO_2 hydrogenation activity of the CuO–ZnO–Ga_2O_3/HZSM-5 catalyst at the optimal temperature of 260 °C.

In view of these observations, each metal component has a unique effect on the system studied in this paper. As stated above, CuO is the active center of methanol reaction in the catalyst of carbon dioxide hydrogenation to dimethyl ether, which causes carbon dioxide hydrogenation to form
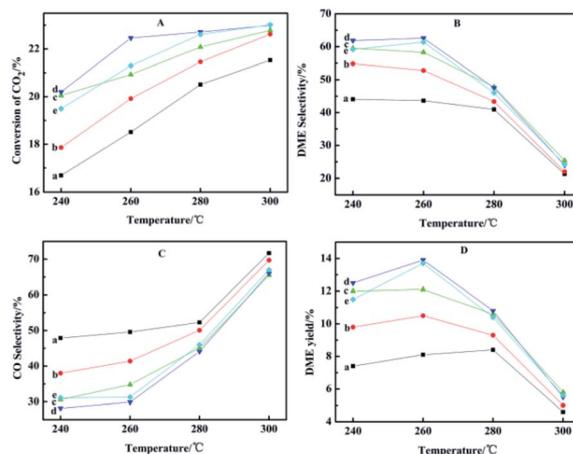
Fig. 8 Effect of reaction temperature on the catalytic performance: (a) CZG_0H; (b) CZG_1H; (c) CZG_3H; (d) CZG_5H; (e) $CZG_{10}H$.

methanol.[48] ZnO can effectively improve the degree of copper dispersion to increase the specific surface area of Cu and increase the stability of the catalyst.[49] The formation of the Zn–CuO alloy from ZnO and CuO is the main active point of methanol synthesis, thus increasing the conversion rate of CO_2.[50] The Ga_2O_3 promoted bifunctional catalyst shows a good dispersion of copper with a small particle size, which leads to a high surface area of copper and an increase in the acidity of dehydrated components. Ga_2O_3 as is used as an electronic promoter to adjust the optimal ratio of Cu^+/Cu^0 in the catalyst.[29] All of these lead to a high rate of methanol formation and continuous dehydration to DME, thus increasing the selectivity to DME.[51]

4. Conclusions

In conclusion, Ga_2O_3 promoted CuO–ZnO–Ga_2O_3/HZSM-5 catalysts for dimethyl ether synthesis from CO_2 hydrogenation were prepared and the catalytic performances were evaluated. An appropriate amount of Ga_2O_3 benefited smaller Cu particles, higher copper surface areas, intensified CuO–ZnO interaction, and proper acid amounts, maintained the proportion of Cu^+/Cu^0 on the surface of the catalyst and acid site distribution, therefore leading to higher CO_2 conversion and DME selectivity. Among the investigated catalysts, the hybrid system CuO–ZnO–Ga_2O_3/HZSM-5 showed the best performance when the content of Ga_2O_3 was 5 wt% in the direct conversion of CO_2 to DME. The CZG$_5$H catalyst showed the maximum CO_2 conversion, DME selectivity and DME yields of 22.3%, 62.6% and 14.0%, respectively, under the reaction conditions of the optimal reaction temperature of 260 °C, the space velocity of GHSV 1500 h^{-1} and the reaction pressure of 3.0 MPa.

Conflicts of interest

The authors declare no conflict of interest.

Acknowledgements

References

1 O. I. Awad, O. M. Ali, R. Mamat, A. A. Abdullah, G. Najafi, M. K. Kamarulzaman, I. M. Yusri and M. M. Noor, *Renewable Sustainable Energy Rev.*, 2017, **69**, 1232–1242.

2 F. A. Rahman, M. M. A. Aziz, R. Saidur, W. A. W. A. Bakar, M. R. Hainin, R. Putrajaya and N. A. Hassan, *Renewable Sustainable Energy Rev.*, 2017, **71**, 112–126.

3 Z. Azizi, M. Rezaeimanesh, T. Tohidian and M. R. Rahimpour, *Chem. Eng. Process.*, 2014, **82**, 150–172.

4 T. H. Fleisch, A. Basu and R. A. Sills, *J. Nat. Gas Sci. Eng.*, 2012, **9**, 94–107.

5 V. N. Ipatieff and G. S. Monroe, *J. Am. Chem. Soc.*, 1945, **67**, 2168–2171.

6 D. M. Sung, Y. H. Kim, E. D. Park and J. E. Yie, *Catal. Commun.*, 2012, **20**, 63–67.

7 S. J. Ren, X. Fan, Z. Y. Shang, W. R. Shoemaker, L. Ma, T. P. Wu, S. G. Li, N. B. Klinghoffer, M. Yu and X. H. Liang, *J. CO$_2$ Util.*, 2020, **36**, 82–95.

8 I. Miletto, E. Catizzone, G. Bonura, C. Ivaldi, M. Migliori, E. Gianotti, L. Marchese, F. Frusteri and G. Giordano, *Materials*, 2018, **11**, 2275.

9 J. Abu-Dahrieh, D. Rooney, A. Goguet and Y. Saih, *Chem. Eng. J.*, 2012, **203**, 201–211.

10 S. Hassanpour, F. Yaripour and M. Taghizadeh, *Fuel Process. Technol.*, 2010, **91**, 1212–1221.

11 H. Bahruji, R. D. Armstrong, J. R. Esquius, W. Jones, M. Bowker and G. J. Hutchings, *Ind. Eng. Chem. Res.*, 2018, **57**, 6821–6829.

12 R. Khoshbin, M. Haghighi and P. Margan, *Energy Convers. Manage.*, 2016, **120**, 1–12.

13 M. Sanchez-Contador, A. Ateka, A. T. Aguayo and J. Bilbao, *Fuel Process. Technol.*, 2018, **179**, 258–268.

14 T. Witoon, P. Kidkhunthod, M. Chareonpanich and J. Limtrakul, *Chem. Eng. J.*, 2018, **348**, 713–722.

15 Q. Zhang, Y. Z. Zuo, M. H. Han, J. F. Wang, Y. Jin and F. Wei, *Catal. Today*, 2010, **150**, 55–60.

16 Y. B. Hu, Y. J. Zhang, J. Du, C. Y. Li, K. J. Wang, L. D. liu, X. R. Yu, K. Wang and N. Liu, *RSC Adv.*, 2018, **8**, 30387–30395.

17 W. J. Cai, Q. Chen, F. G. Wang, Z. C. Li, H. Yu, S. Y. Zhang, L. Cui and C. M. Li, *Catal. Lett.*, 2019, **149**, 2508–2518.

18 J. Słoczyński, R. Grabowski, P. Olszewski, A. Kozłowska, J. Stoch, M. Lachowska and J. Skrzypek, *Appl. Catal., A*, 2006, **310**, 127–137.

19 S. Natesakhawat, J. W. Lekse, J. P. Baltrus, P. R. Ohodnicki, B. H. Howard, X. Y. Deng and C. Matranga, *ACS Catal.*, 2012, **2**, 1667–1676.

20 G. Bonura, C. Cannilla, L. Frusteri and F. Frusteri, *Appl. Catal., A*, 2017, **544**, 21–29.

21 H. Ham, S. W. Baek, C. H. Shin and J. W. Bae, *ACS Catal.*, 2019, **9**, 679–690.

22 Q. Jiang, Y. F. Liu, T. Dintzer, J. J. Luo, K. Parkhomenko and A. C. Roger, *Appl. Catal., B*, 2020, **269**, 118804.

23 Y. Q. Zhao, J. X. Chen and J. Y. Zhang, *J. Nat. Gas Chem.*, 2007, **16**, 389–392.

24 Q. Sun, Y. L. Zhang, H. Y. Chen, J. F. Deng, D. Wu and S. Y. Chen, *J. Catal.*, 1997, **167**, 92–105.

25 Y. J. Lee, M. H. Jung, J. B. Lee, K. E. Jeong, H. S. Roh, Y. W. Suh and J. W. Bae, *Catal. Today*, 2014, **228**, 175–182.

26 J. Toyir, P. R. de la Piscina, J. L. G. Fierro and N. Homs, *Appl. Catal., B*, 2001, **29**, 207–215.

27 K. W. Jun, W. J. Shen, K. S. R. Rao and K. W. Lee, *Appl. Catal., A*, 1998, **174**, 231–238.

28 Y. Q. Sun, X. H. Han and Z. K. Zhao, *Catal. Sci. Technol.*, 2019, **9**, 3763–3770.

29 J. Toyir, P. R. de la Piscina, J. L. G. Fierro and N. Homs, *Appl. Catal., B*, 2001, **34**, 255–266.

30 P. B. Sanguineti, M. A. Baltanas and A. L. Bonivardi, *Appl. Catal., A*, 2015, **504**, 476–481.

31 C. J. Xu, X. Y. Hao, M. Y. Gao, H. Q. Su and S. H. Zeng, *Catal. Commun.*, 2016, **73**, 113–117.

32 S. Kuhl, J. Schumann, I. Kasatkin, M. Havecker, R. Schlogl and M. Behrens, *Catal. Today*, 2015, **246**, 92–100.

33 S. Asthana, C. Samanta, R. K. Voolapalli and B. Saha, *J. Mater. Chem. A*, 2017, **5**, 2649–2663.

34 L. Y. Li, D. S. Mao, J. Xiao, L. Li, X. M. Guo and J. Yu, *Chem. Eng. Res. Des.*, 2016, **111**, 100–108.

35 R. W. Liu, Z. Z. Qin, H. B. Ji and T. M. Su, *Ind. Eng. Chem. Res.*, 2013, **52**, 16648–16655.

36 C. M. Li, X. D. Yuan and K. R. Fujimoto, *Appl. Catal., A*, 2014, **469**, 306–311.

37 F. C. F. Marcos, J. M. Assaf and E. M. Assaf, *Mol. Catal.*, 2018, **458**, 297–306.

38 F. P. Li, M. Ao, G. H. Pham, J. Sunarso, Y. P. Chen, J. Liu, K. Wang and S. M. Liu, *Small*, 2020, **16**, 1906276.

39 V. Deerattrakul, P. Dittanet, M. Sawangphruk and P. Kongkachuichay, *J. CO₂ Util.*, 2016, **16**, 104–113.

40 A. M. Hengne, D. J. Yuan, N. S. Date, Y. Saih, S. P. Kamble, C. V. Rode and K. W. Huang, *Ind. Eng. Chem. Res.*, 2019, **58**, 21331–21340.

41 L. M. He, X. R. Li, W. W. Lin, W. Li, H. Y. Cheng, Y. C. Yu, S. I. Fujita, M. Arai and F. Y. Zhao, *J. Mol. Catal. A: Chem.*, 2014, **39**, 143–149.

42 P. H. Matter, D. J. Braden and U. S. Ozkan, *J. Catal.*, 2004, **223**, 340–351.

43 K. P. Sun, W. W. Lu, F. Y. Qiu, S. W. Liu and X. L. Xu, *Appl. Catal., A*, 2003, **252**, 243–249.

44 K. Klier, *Adv. Catal.*, 1982, **31**, 243–313.

45 G. Celik, A. Arinan, A. Bayat, H. O. Ozbelge, T. Dogu and D. Varisli, *Top. Catal.*, 2013, **56**, 1764–1774.

46 S. J. Ren, W. R. Shoemaker, X. F. Wang, Z. Y. Shang, N. Klinghoffer, S. G. Li, M. Yu, X. Q. He, T. A. White and X. H. Liang, *Fuel*, 2019, **239**, 1125–1133.

47 G. Bonura, M. Migliori, L. Frusteri, C. Cannilla, E. Catizzone, G. Giordano and F. Frusteri, *J. CO₂ Util.*, 2018, **24**, 398–406.

48 S. Kattel, P. J. Ramírez, J. G. Chen, J. A. Rodriguez and P. Liu, *Science*, 2017, **355**, 1296–1299.

49 J. Nakamura, T. Uchijima, Y. Kanai and T. Fujitani, *Catal. Today*, 1996, **28**, 223–230.

50 T. Fujitani and J. Nakamura, *Appl. Catal., A*, 2000, **191**, 111–129.

51 S. H. Kang, J. W. Bae, H. S. Kim, G. M. Dhar and K. W. Jun, *Energy Fuels*, 2010, **24**, 804–810.